Wireless Networks
https://doi.org/10.1007/s11276-023-03533-z

ORIGINAL PAPER

PP-based 24 GHz wearable antenna

María Elena de Cos Gómez[1] · Humberto Fernández Álvarez[1] · Fernando Las-Heras Andrés[1]

Accepted: 21 September 2023

Abstract

A wearable millimetre-wave radar antenna operating in 24.05–24.25 GHz for imaging applications in collision avoidance to assist visually impaired people is presented. Non-uniform excitation for the series end-fed 1 × 10 array antenna is optimized in simulation achieving a modified Dolph–Chebyshev distribution, which provides improved performance in terms of beam width, Side-lobe level and Gain. Commercial RO3003 and eco-friendly polypropylene (PP) are considered as substrates for comparison purposes, being the PP electromagnetically characterized for the first time at such high frequencies. Consistent agreement between simulation and measurement results is achieved for antenna prototypes on both dielectrics. The impedance matching bandwidth is analysed for the antenna on PP also under bent conditions. The overall size of the compact, low-cost, eco-friendly and flexible antenna on PP is 98.68 × 14.4 × 0.52 mm^3 and, according to literature survey, it overcomes the state of the art on wearable radar antennas at 24 GHz.

Graphical Abstract

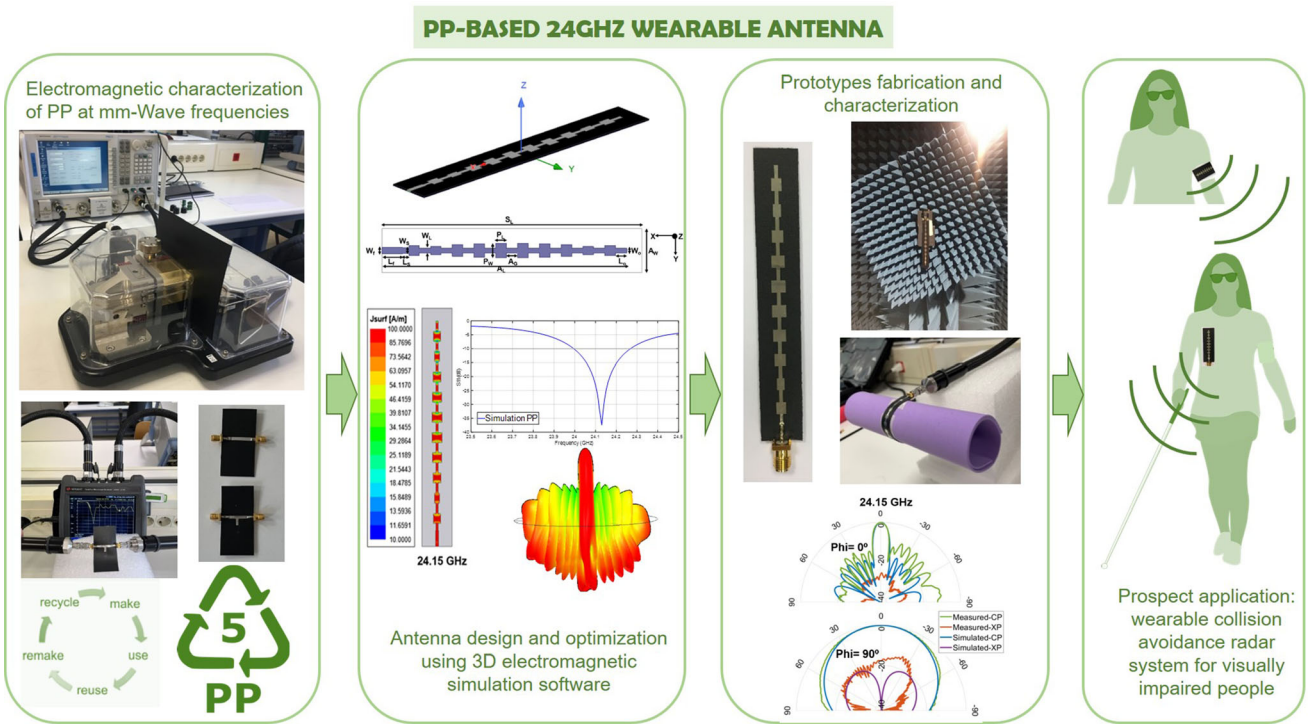

Keywords Wearable · Polypropylene · Antenna · Radar · mm-Wave · Collision avoidance

✉ María Elena de Cos Gómez
medecos@uniovi.es

[1] Área de Teoría de La Señal y Comunicaciones. Dpt. Ingeniería Eléctrica, Universidad de Oviedo. Edificio Polivalente, Mod. 8, 33203 Gijón, Asturias, Spain

Published online: 16 October 2023

1 Introduction

The main resource for assisting blind people has been the white cane, sometimes supplemented by the guide dog, which has to be trained specifically for this purpose. However, these methods do not provide full autonomy [1, 2], as they do not protect the upper body from collisions. This is why a number of electronic travel aid (ETA) systems have emerged in recent years. Although ultrasonic sensing systems have been widely used because of their low cost [3], they nevertheless have difficulties in detecting smooth surfaces as well as narrow openings (e.g., half-open doors or windows), due to their broad radiation pattern [4, 5]. Systems based on infrared sensors have the drawback of requiring direct visibility between the sensors [6]. In addition, systems based on Near-Field communications (NFC) are accurate only in very short distances [6]. Optical technologies (e.g., cameras) have also been postulated as ETAS, but they are very sensitive to natural light which limits their resolution and are inoperative in low visibility conditions (e.g., due to fog) [7]. Therefore, the proposed systems are not sufficient to provide safe mobility, given their limitations in scope or accuracy, and even in cost. Sometimes a combination of technologies has been encouraged [5, 8], resulting in complex and/or more expensive systems. It is also important to mention that ETA systems must be light, comfortable and compact, to facilitate their continued daily use, and that it is essential that the cost of the complete system be affordable. In the absence of a robust technology for ETA application, the mmWave radar-based systems have been developed in recent years, due to the advantages of this technology in terms of scope, accuracy, and operation capacity in all environmental conditions. In [9], for example, a portable vector network analyzer (VNA) is used for testing the detection either indoor or outdoor scenarios. The system was able to detect more than one obstacle. A frequency-modulated continuous wave radar-based system operating at the center frequency of 80 GHz and situated at the head of a blind person is presented in [10]. This sensor scans the surrounding of the user and detects the position of obstacles up to 5 m. Furthermore, the use of natural movement to create a synthetic aperture and, therefore, improving the resolution has also been proposed in [11, 12]

In collision avoidance applications, the radar detects the range and speed of objects near the person or the vehicle whose integrity is to be protected. The radar consists of a transceiver. The transmitter emits radio waves that knock the body of the object or target and spring back to the receiver, being used to determine the speed, distance, and direction of the object [13, 14].

The antenna of the radar has a great impact on its performance [15]. When illuminating the whole scenario at a time at a short distance, a wide beam is preferable for simple detection. The angular determination of the target is however determined by the directivity of the antenna [16]. By measuring the direction in which the antenna is pointing when the echo is received, both the azimuth and elevation angles from the radar to the object or target can be determined. The accuracy of angular measurement is determined by the directivity, which is a function of the antenna size. Thus, depending on the envisioned application a trade-off solution between coverage area and range has to be adopted [15].

Radar units usually work with very high frequencies since they enable high resolution (the smaller the wavelength, the smaller the detectable objects) and more compact sizes (the higher the frequency, the smaller the antenna size at the same gain). For example, 24 GHz radars have been used for industrial control, pedestrian recognition [17], security and biomedical applications [18].

The European Telecommunications Standards Institute (ETSI) has a temporary standard [19] from 24.05 to 24.25 GHz for Short Range Radar (SRR). Besides, the 24.125 GHz Industrial Scientific and Medical (ISM) license free band also ranges from 24.05 to 24.25 GHz. Moreover, both the Federal Communications Commission (FCC) and ETSI have a license free Ultra WideBand (UWB) frequency band in this range (between 22–29 GHz in the US and 22.65–25.65 GHz in Europe), which can also be used for collision avoidance radar applications. The 77 GHz band, on the other hand, is intended to applications that require long range, such as automotive cruise control [20, 21]. It should not be overlooked that it has technological disadvantages compared to the 24 GHz band, in terms of manufacturing impairments, even using conventional dielectrics [20]. Therefore, aiming at exploring the use of new materials in mm-wave frequencies, it does not seem to be the suitable choice.

For the intended application of a collision avoidance system devoted to assist visually impaired people, at a medium distance, it is required to achieve an antenna with a narrow beam and low side-lobe level (SLL). In addition, the antenna should be compact, lightweight and comfortable to wear, in order to provide safety in the mobility of the system users without detriment to their comfort, thus improving the quality of life of the target users.

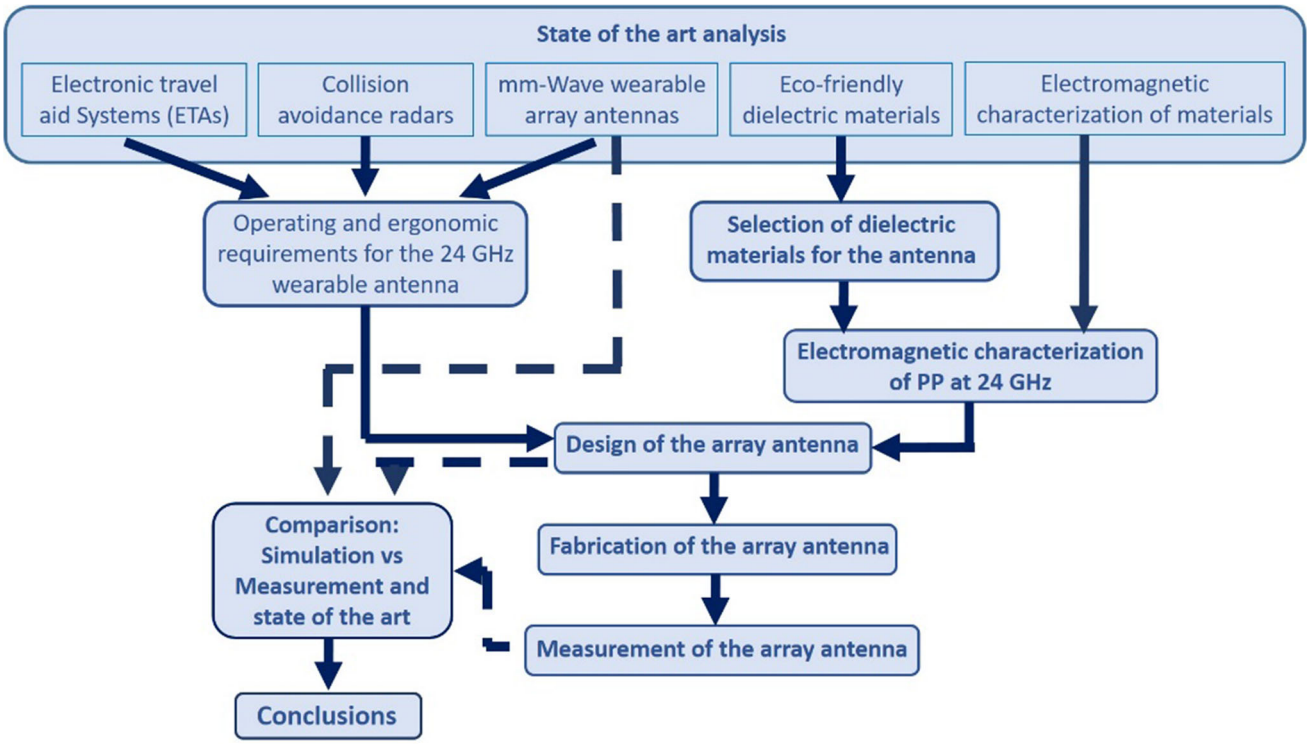

Fig. 1 Flowchart describing the steps followed in the research

Antenna arrays provide higher gain and directivity than individual antennas [22, 23]. Furthermore, a common technique to suppress the side-lobe level and improve the directivity in such arrays is non-uniform excitation [24]. Analytical methods for sum patterns such as Chebyshev or Taylor polynomials are widely used for uniformly spaced linear arrays with isotropic elements. To achieve equal leveled side lobes, Dolph originally introduced Chebyshev polynomials for the excitation of isotropic antenna arrays [25]. Previous literature contributions have outlined the design procedure of purely Dolph–Chebyshev (DC) based arrays [26–30] with optimal compromise between side lobe level (SLL) and main lobe width. The DC patterns exhibit many advantages such as controlled SLL or trade-off between SLL and number of elements. However, either beam width or SLL can be used as a design parameter, not both. Therefore, optimized modifications of the aforementioned DC synthesis are of high interest. Depending on the intended application for the radar system, the geometric parameters of the antenna should be optimized in simulation, through parametric analysis, to meet the impedance matching band requirements and radiation properties for optimal operation.

Nowadays there is a growing interest in communication systems with a reduced ecological footprint. Furthermore, antennas for wearable systems or those to be integrated into devices should be light, flexible, ergonomic and low cost. From these premises comes the interest in using materials such as Polypropylene (PP), which in addition, has not been used in frequencies as high as millimetre wave band and it is unknown how the material behaves regarding its possibilities of use for the manufacture of antennas. Therefore, electromagnetic characterization in such a band is essential and constitutes a challenge. It is also a great achievement to manufacture antennas using such unconventional materials, even more so considering the reduced dimensions of the resulting designs.

In this contribution, a wearable array antenna optimized to be used in a 24 GHz radar system for collision avoidance system is presented. Such system is applicable, for example, to increase the safety of blind people. Sustainable and flexible polypropylene (PP) is used for the first time as a dielectric substrate for an antenna at millimetre wave frequencies. This adds to the designed antenna not only ergonomic and flexibility advantages, but also contributes to reducing manufacturing costs and contributes to a

circular economy, thereby reducing the ecological footprint of the system.

In accordance with the flowchart describing the steps followed in the research and shown in Fig. 1, the rest of the manuscript is organized as follows: first, the dielectric substrates considered for the design of the antenna are presented. Then the electromagnetic characterization of the polypropylene (PP) at the intended millimeter wave frequency is addressed. Next, the design of the optimized array antenna is conducted on both conventional RO3003 and PP for comparison. Prototypes of the antenna on both dielectrics are fabricated and characterized in terms of impedance matching and radiation properties. Moreover, the impedance matching of antenna on PP is measured under bent conditions. Then comparison with the state of the art is conducted to support the advantages of the presented antenna on PP. Finally, some conclusions are drawn.

2 Dielectric substrates for the design of the antenna

Two substrates are considered for the design of the antenna: commercial substrate Rogers' RO3003, which is widely used in electronics, and polypropylene (PP), not conventionally used as an electronics substrate and even less at millimetre wave frequencies.

RO3003 [31] exhibits certain degree of conformability and softness so that it can be used in wearable devices. It is extensively used for Microwave and RF electronics due to its good electrical and mechanical properties, along with a competitive price. Its composition, consisting of ceramic-filled PTFE (Teflon) composites, endows it with advantageous properties: very stable relative dielectric permittivity with temperature, $\varepsilon_r = 3.0$, and very low loss tangent, $\tan\delta = 0.0013$. However, although its process is free of heavy metals and therefore compliant with Restriction of Hazardous Substances (RoHS) regulation [32], like many other commercial substrates, it cannot be considered eco-friendly, precisely because it is based on PTFE.

Polypropylene (PP) is extensively used in food packaging, medical and automotive applications, among others, because of its flexibility, lightness, resistant to fatigue and environmental benefits [33]. It is a recyclable thermoplastic polymer aligned with the circular economy principles and it does not release as many toxins and CO as other plastics such as PVC, PET and PS. It can be recycled multiple times [34–36].

The pioneering use of PP for antennas in the 2.4 GHz band [37] for wireless communications (such as WIFI, ZigBee, bluethood, RFID, and others) has been successfully followed by several authors for applications in microwave bands [38–43]. However, its use at higher frequencies, such as mm-wave frequencies is a great challenge, since at high frequencies the dimensions of the antennas are reduced, it is necessary to optimize the manufacturing procedures (even more so on a material that is not used for that purpose) and the behaviour of the material from the point of view of its electromagnetic properties is unknown (which totally conditions the result from the design stage, since the data must be entered into the electromagnetic simulation software). At high frequencies, a small variation in the dimensions of the antenna can shift the operating band considerably, rendering the resulting antenna useless.

3 Electromagnetic characterization of the polypropylene at millimetre wave frequencies

The first step when approaching the design of an antenna, on a dielectric substrate that has not been used in a certain frequency band before and that in addition is not a commercial material used for this purpose, is to carry out the electromagnetic characterization of the dielectric, in the band of interest for the operation of the antenna, with suitable methods. If the electromagnetic characterization of the dielectric is not accurate, this will result in significant mismatches in the behavior of the antenna once manufactured with respect to that expected from its simulation-based design. Thus, variations in the value of the relative dielectric permittivity ε_r will cause shifts in the antenna operating band, while variations in the loss tangent $\tan\delta$ will influence the impedance matching of the antenna and its radiation parameters.

The vast majority of commercial dielectrics for antenna design are characterized at frequencies of 1 GHz or, at most, 10 GHz. Of course, for general-purpose circuitry, data in the MHz range is also usually provided. Therefore, it is not surprising that 10 GHz split cylinder resonant cavities are available to carry out a very precise but narrow-band characterization [44]. This method is intended for rigid substrates [45, 46]. Measurements can be made at higher frequencies, using higher cavity modes at the cost of losing precision in the results. There are also coaxial probe-based broadband characterization methods that are slightly less accurate, but can be used more easily for materials that are not rigid [47]. The use of devices based on suspended

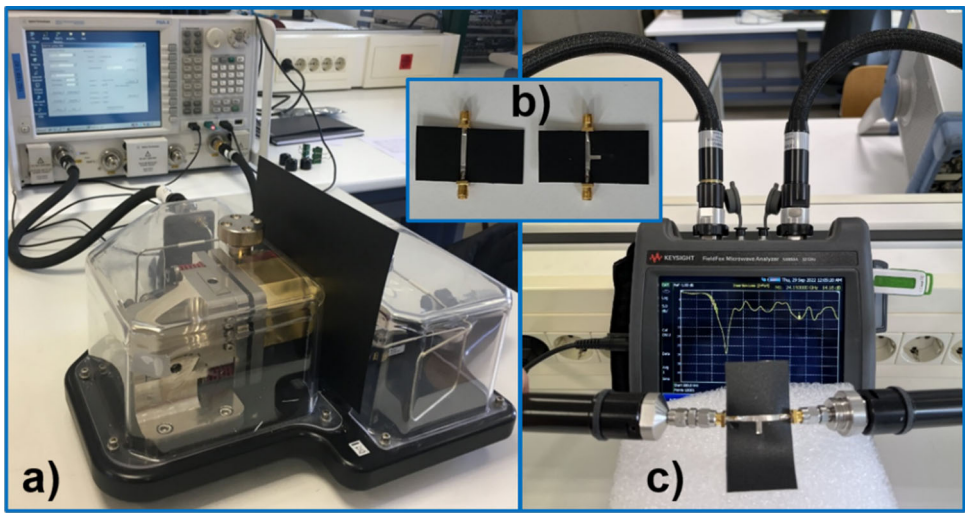

Fig. 2 Electromagnetic characterization of the PP at about 24 GHz: **a** split-cylinder resonator; **b** microstrip line and T-resonator samples; **c** measurement set-up for the S-parameters

microstrip lines and split-post dielectric resonators for certain frequency ranges has also proven useful in several works, although they are designed for specific sample thicknesses, which greatly limits their use [48]. Free space methods are broadband and probed useful to characterize the materials [49] but do not include the effects derived from fabrication, which are key to avoid frequency shifts in the operation band of the prototypes compared to the simulation results.

Other authors have provided characterization methods based on microstrip lines [50, 51] and different types of resonators (rings, stubs in open circuit and others) [52–54] that have the advantages of being specifically designed for the frequency band of interest, and that they are implemented directly on the dielectric under study, with the same manufacturing technique as the antenna (thereby incorporating possible tolerances which, with another method, would have to be dealt with later). The characterization is carried out by finding the necessary relative dielectric permittivity and loss tangent values, in simulation, so that the results conform to those obtained in measurement for identical structures (microstrip lines and resonator).

In this work, both measurements with a 10 GHz resonant cavity (see Fig. 2(a)), also with higher modes in the band around 24 GHz, as well as the method based on microstrip lines and on resonant stub in open circuit in such band, are used to obtain a characterization of the polypropylene (PP) that is as accurate as possible for the purpose of this work: designing an array-type antenna with microstrip feeding.

Several measurements were conducted using higher order modes of the split cylinder resonant cavity [44] (Keysight Technologies 85072A) around 24 GHz (more specifically at 25 GHz) for a sample with thickness h = 0.52 mm and then statistical treatment of the retrieved data was carried out. The resulting relative dielectric permittivity and loss tangent are respectively: $\varepsilon_r = 2.42$ and $\tan\delta = 0.002$. These values should be considered as a first step in the characterization. The fabricator of the resonant cavity recommends using samples in the 0.1–3 mm range, and typically 1 mm [44]. The smaller the thickness of the sample, the lesser disturbance it causes in the reference resonance frequency and the higher the inaccuracy, since the disturbance is the base of the characterization method.

The estimated value obtained with the split cylinder resonant cavity was used as a starting point of the microstrip based method [52], which refines the characterization and includes potential over-etching and under-etching effects that occurs in the fabrication of the antenna. Two microstrip lines of identical characteristic impedance are required: a simple line and a line with a $\lambda g/4$ stub (T-resonator) at the intended characterization frequency. Both lines are fabricated and subsequently their S21 parameter is simulated using HFSS, tuning ε_r and $\tan\delta$ in the simulation to match the measurement results obtained with a vector network analyser (see Fig. 2(c). It is important to indicate that, since at millimeter frequencies a $\lambda g/4$ stub is very short (and there would be a high coupling with the line itself), it is better for practical purposes to use sizes 3 $\lambda g/4$ and/or 5 $\lambda g/4$ and consider the corresponding resonance. Tests were performed with both lengths. Figure 2(c) shows

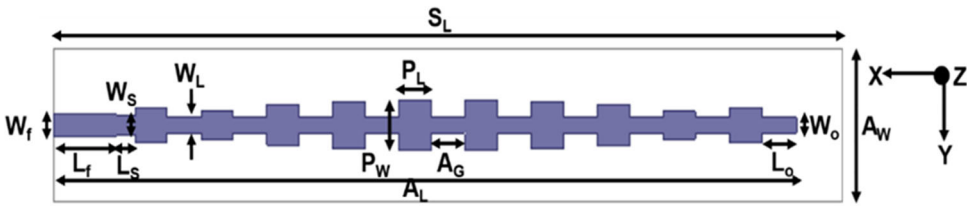

Fig. 3 Geometry of the series-fed DC inspired microstrip patch array antenna

Table 1 Dimensions of the array antenna for different dielectric substrates

Substrate	Dimensions (mm)													
	S_L	A_W	A_L	h	W_f	L_f	L_S	W_S	W_L	P_W	P_L	A_G	L_o	W_o
RO3003	86.8	14.4	80.8	0.762	2.06	6	2	1.76	1.5	4.8	3.52	3.75	3.85	1.5
PP	98.68	14.4	92.68	0.52	1.61	6	3	1	1.3	4.8	4.15	4.22	4.2	1.3

the result obtained in the measurement for 3 λg/4. In addition, the width of the microstrip line used is 2.5 mm, which does not correspond exactly to an impedance of 50Ω, for which a certain ripple can be seen in the measurement. This is not an obstacle to the method as long as identical dimensions are used in the simulation to retrieve the values. As a result of carrying out this method $\varepsilon_r = 2.2$ and $\tan\delta = 0.002$ were obtained at 24.6 GHz.

Moreover, a simple microstrip-fed patch antenna at 24.15 GHz (central value of the intended frequency band) was designed and tested using the later retrieved values. Measurement results of the S11 agreed very well with the simulation ones, so that it can be considered that those values are the proper ones to be considered for design at this frequency range.

4 Design of the array antenna

Series feeding, consisting of a continuous transmission line through which a proportion of energy is progressively coupled into each element of an array along the line, has been chosen. It has advantages over the corporate feed in that its structure is simpler, it occupies less space, and above all, it exhibits lower losses and provides higher radiation efficiency as the number of array elements increases [55]. It can be seen as a travelling wave transmission line, where fractions of power are coupled into each single element, being the amplitude of the excitation controlled through the variation of the widths of the patches and/or feeders and the phase by adjusting the patches spacing.

The array is composed of 10 patch elements and has bilateral symmetry but for the feeding line (see Fig. 3). The length of the patches (P_L) is uniform and approximately equal to half the guided wavelength at the central frequency of the operating band (24.05–24.25 GHz). To reduce the side-lobe level the width of the patches (P_W) is tapered, following a decreasing sequence or ratio from the initially optimized central patches, to acquire a non-uniform excitation. In the first step, the width tapering follows a purely Dolph–Chebyshev (DC) approach. Then the coefficients of the polynomial are modified by sweeps conducted in simulation, until obtaining optimal values that provide the desired behaviour for the antenna, both in impedance matching and radiation pattern properties. In addition, an open-ended stub is introduced at the last element to get a constant current flowing through all the antenna elements and an efficient use of transmitted power. The length of the open stub is a half guided wavelength at the operating central frequency. The spacing between two adjacent patch antenna elements (A_G), and thus the length of the transmission line between patches, is identical and is about half the guided wavelength at the central frequency of the operating band.

Table 2 Power ratio from the center patch to edge of the array antenna

P1	P2	P3	P4	P5
1	0.92	0.8	0.55	0.7

The total length of the array is A_L, whereas the overall PCB length and width are respectively S_L and A_W.

The detailed dimensions of the optimized array antenna for RO3003 and PP substrates are shown in Table 1 and the patch width ratio from the center patch to edge are indicated in Table 2.

The S11(dB) obtained in simulation for the optimized dimensions and power ratio is shown in Fig. 4. Very good matching is achieved for the target frequency band 24.05–24.25 GHz for both RO3003 and PP. The specific

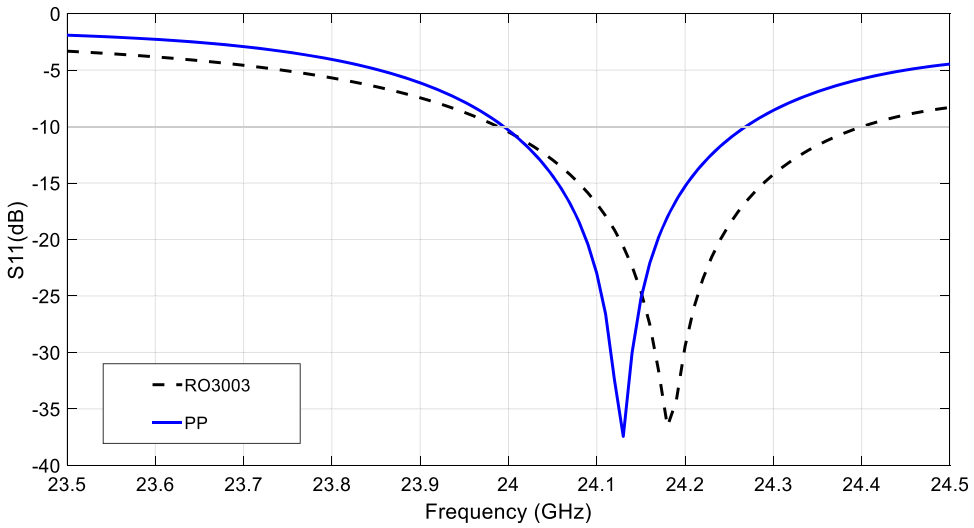

Fig. 4 Reflection coefficient results, S11 (dB), in simulation for the antenna on RO3003 and PP

Table 3 Frequency bands and bandwidths of the array antenna on different substrates

Substrate	Frequency band			
	Freq (GHz)		Bandwidth	
	f_{Low}	f_{Up}	Total (MHz)	%
RO3003	23.98	24.40	420	1.73
PP	23.99	24.27	280	1.16

matching bandwidth is further indicated in Table 3. The result obtained is expected, since although RO3003 has a slightly higher relative dielectric permittivity than PP, the thickness is considerably higher (0.762 mm compared to 0.52 mm), so it provides greater bandwidth. In any case, both cover the band of interest and it is not necessary to exceed it, but try to achieve other advantages such as lightness, flexibility, efficiency and lower cost, which are essential for the intended application.

Fig. 5 shows the surface current distribution for the array antenna at three different frequencies: at the center frequency of the operating band (24.15 GHz) with the expected distribution almost identical for all the array patches with high current level at the center and decreasing to the edges in the X (feeding) direction, indicating than all of them contribute to the antenna operation, and at two non-operating frequencies (23.3 and 25.6 GHz) which do not match a mode of the patches and it is different from one patch to another, depending on its position.

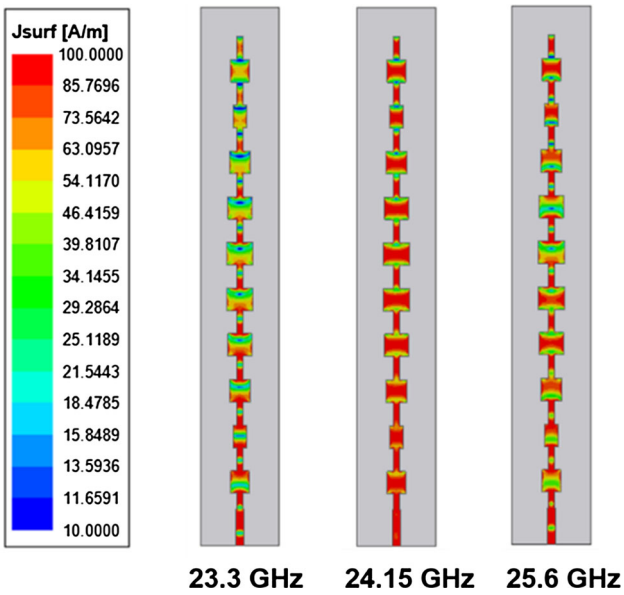

Fig. 5 Surface current distribution for the array antenna on PP at 23.3, 24.15 and 25.6 GHz

Regarding the radiation properties of the array antenna, Table 4 indicates the peak realized gain (G), peak directivity (D), radiation efficiency (η) and front to back ratio (FTBR) obtained in simulation for the center and edge frequencies of the target band. In addition, the side-lobe level (SLL) and half-power beam width (HPBW), for the pattern cuts Phi = 0° and Phi = 90° at the center frequency, are also provided. With both materials, suitable properties

Table 4 Radiation properties results obtained in simulation

	Freq (GHz)	G (dBi)	D (dB)	η (%)	FTBR (dB)	SLL (dB) φ = 0°	HPBW (°) φ = 0°	SLL (dB) φ = 90°	HPBW (°) φ = 90°
RO3003	24.05	15.5	15.8	93	26.2	− 14	11.6	− 25	61
	24.15	15.5	15.6	98	23.9				
	24.25	15.1	15.2	98	20.6				
PP	24.05	16.6	17.1	89	26.4	− 18	9.2	− 25	64
	24.15	16.8	17.2	91	25.7				
	24.25	16.4	17.1	85	24.5				

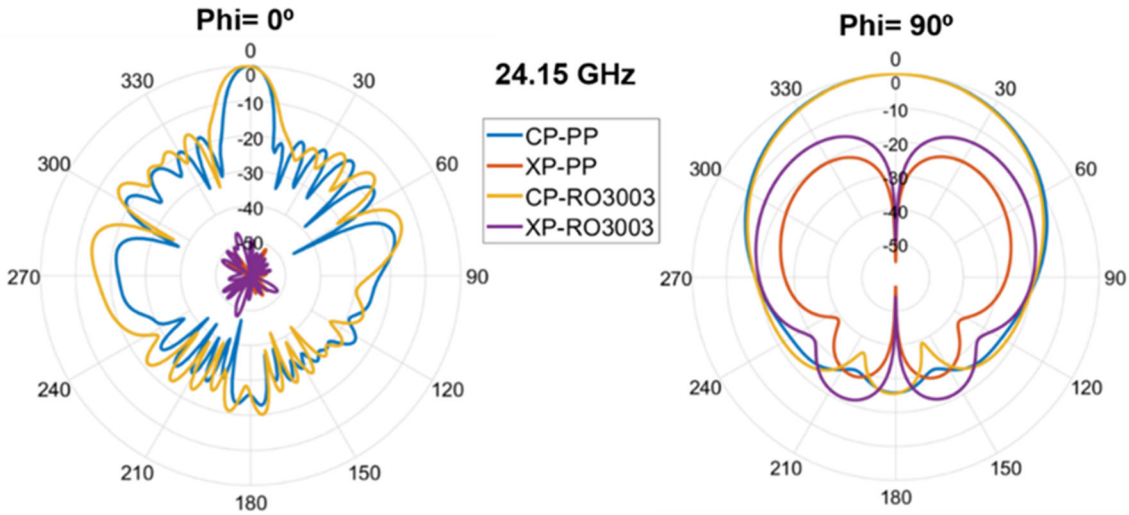

Fig. 6 Radiation Pattern cuts for Phi = 0° and Phi = 90° at 24.15 GHz for PP and RO3003 in simulation

are obtained for the intended application. Especially for PP, which shows even better performance than RO3003 in terms of Gain, directivity, FTBR, SLL and HPBW for Phi = 0°, and almost identical for Phi = 90°. The radiation efficiency, which is a key parameter for wireless devices is very high (≥ 85%) for both dielectrics. The FTBR is also critical for wearables and is better for PP than for RO3003. Furthermore, as it can be observed in Fig. 6, PP provides lower XP level tan RO3003, especially for Phi = 90°. In addition, PP is flexible, recyclable and its cost is much lower than that of RO3003. Thus, PP is much more advantageous than RO3003 for the intended application and the modified DC distribution probes to be a good trade-off solution to achieve the intended antenna performance.

5 Characterization of the array antenna

RO3003 was purchased metallized with copper on both sides. The PP was metallized by fixing to both sides of the sheet a 35 μm thick tin-copper (Sn/Cu) alloy foil that incorporates an adhesive backing. Conventional laser micromachining, with LPKF protolaser machine, was used to fabricated both antennas. Feeding SMA connectors operating up-to 26 GHz were soldered by hand (see Fig. 7).

Simulation and measurement of the reflection coefficient are in good agreement (see Fig. 7), especially for the PP, and both prototypes exhibit proper impedance matching in the target band (24.05–24.25 GHz). It has to be noted that

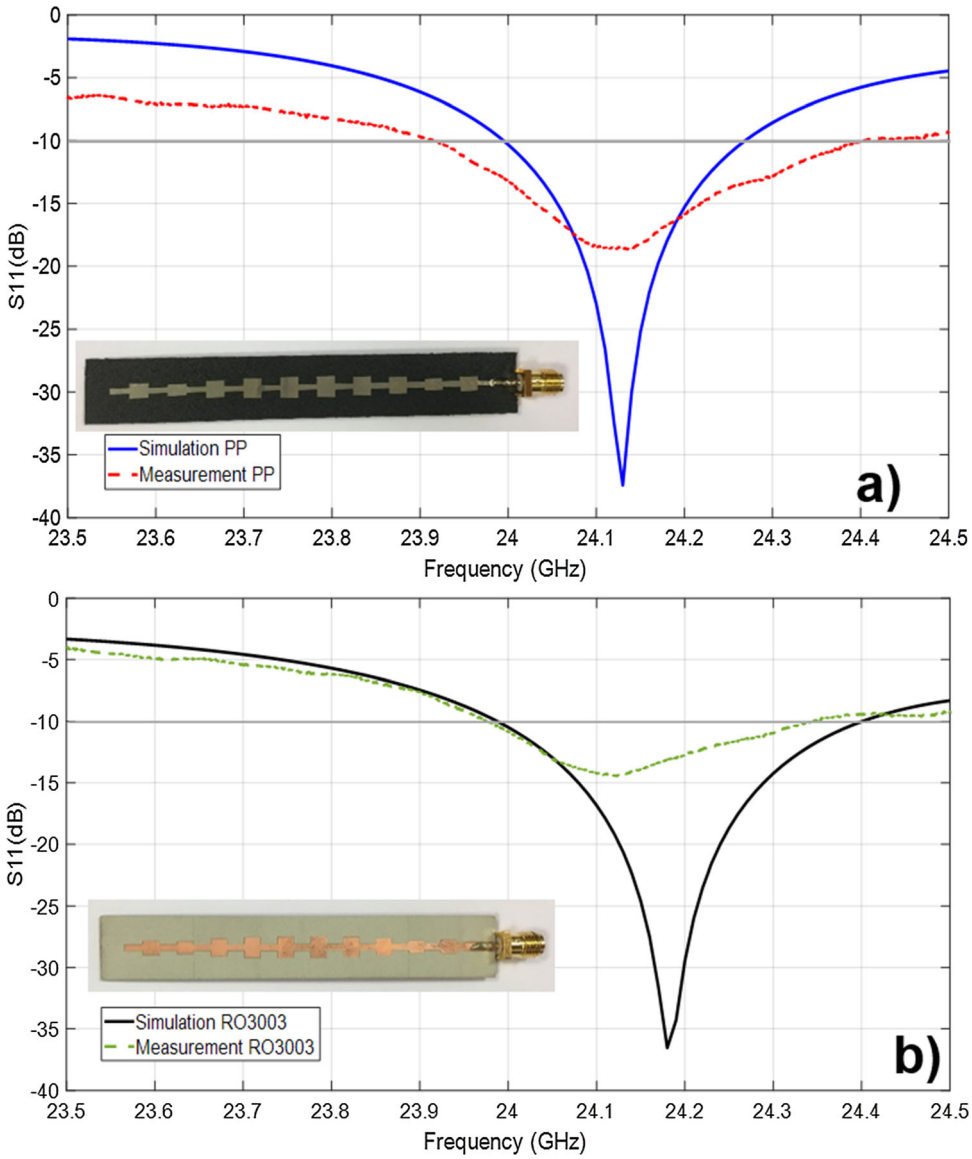

Fig. 7 Measurement results of the reflection coefficient, S11 (dB), for the fabricated array antenna: **a** on copper plated PP and **b** on copper plated RO3003, versus the simulation results

the connector was not included in simulation and was soldered by hand, so that disturbances can be attributed to that fact.

Fairly good agreement is achieved between simulation and measurement results of the radiation pattern cuts at 24.15 GHz (see Fig. 8), especially for the CP components. HPBW level almost perfectly matches whereas the SLL slightly worsens in measurement for Phi = 0°. The connector was not considered in simulation and it was soldered by hand. Both the cable and the connector can severely perturb the current distribution on the small antenna, and be responsible for the observed XP levels in measurement. Moreover, the 3D printed polylactic Acid (PLA) based piece used to fix the antenna for the measurement, can cause reflections.

The peak realized gain was measured through the gain transfer method, by inter-comparison of the array antenna prototype (antenna under test, AUT), with a Flann Microwave Standard horn 20240-25 (Probe antenna of known characteristics). G = 13 dBi and G = 12.5 dBi were

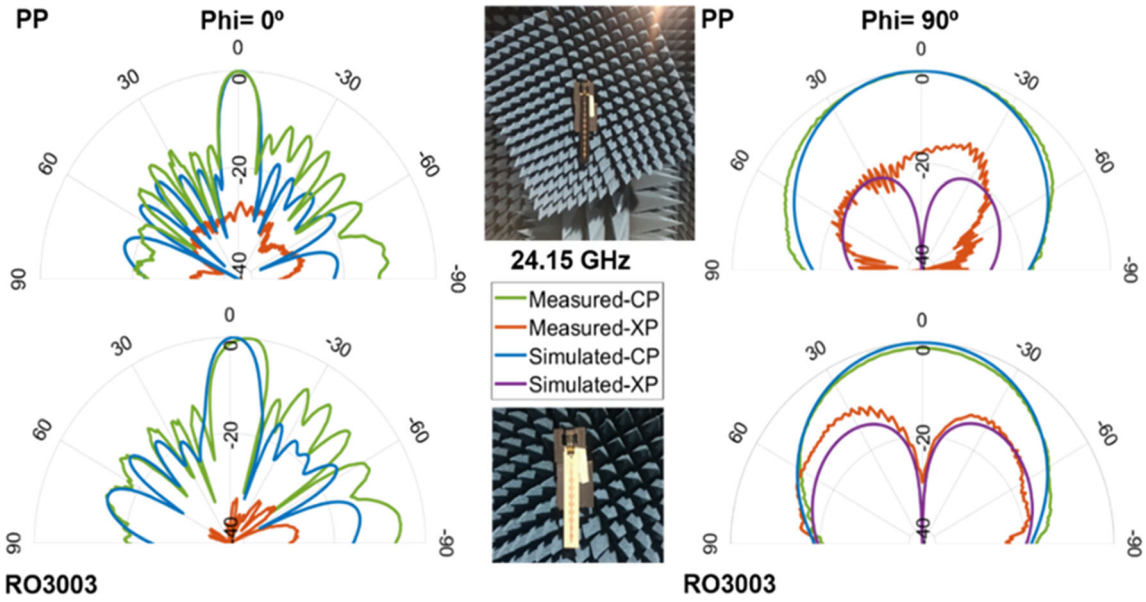

Fig. 8 Simulation vs measurement Radiation Pattern cuts for Phi = 0° and Phi = 90° at 24.15 GHz for PP and RO3003

obtained for the PP and the RO3003 at 24.15 GHz, which are lower than in simulation. Apart from the aforementioned effects of the cable and the connector, the gain measurement can be disturbed by other effects [56]: multipath and reflections due to the fixing PLA structure and other set-up elements, misalignment of AUT-probe and impedance mismatch of antennas.

The directivity calculated using the Krauss approximation [57] considering the HPBW levels from the radiation pattern cuts for Phi = 0° and Phi = 90°, is D = 17.6 dB, and D = 16.5 dB using the Elliot correction [58] for the antenna on PP. For the antenna on RO3003, D = 17.0 dB and D = 16.0 dB are respectively obtained. In both cases the results agree very well with the simulation ones.

The S11 of the antenna on PP was measured under bending conditions in X direction. Two foam cylinders with radius R = 30 mm and R = 22.5 mm were used for such purpose (see Fig. 9). The antenna behaviour under bending conditions is quite robust, even if the impedance matching band widens and the frequency slightly shifts upwards, and it seems that the bending conditions should be extreme to significantly perturb its performance in terms of matching. Nonetheless, the antenna keeps proper matching at the intended frequency band. Moreover, if the antenna is arranged in the front part of clothes, it would not suffer such degree of bending.

6 Comparison with the state of the art

The impedance matching and radiation properties of state of the art array antennas operating at 24 GHz [59–75] are indicated in Tables 5 and 6, as well as their dimensions and dielectric properties. Confronted to antennas on dielectrics with higher ε_r and not eco-friendly, the presented antenna on PP provides higher gain than [59, 61, 63–65] and [68–70], being smaller in terms of area than [61] and overcoming [68] and [70] in terms of HPBW for Phi = 0° and Phi = 90°. It is also smaller than [60, 62, 66] and [67] while providing the same bandwidth than [60] and [67], covering the target 24.05–24.25 GHz band. Furthermore, it provides almost identical bandwidth and radiation properties than a commercial antenna [67] much larger, thicker, heavy, expensive and not suitable for wearable applications.

As for designs on dielectrics with ε_r closer to the PP one, the proposed antenna is much smaller than [71] and [73] for similar bandwidth. It is much thinner and lighter than [72] which is a multilayer complex wideband antenna with

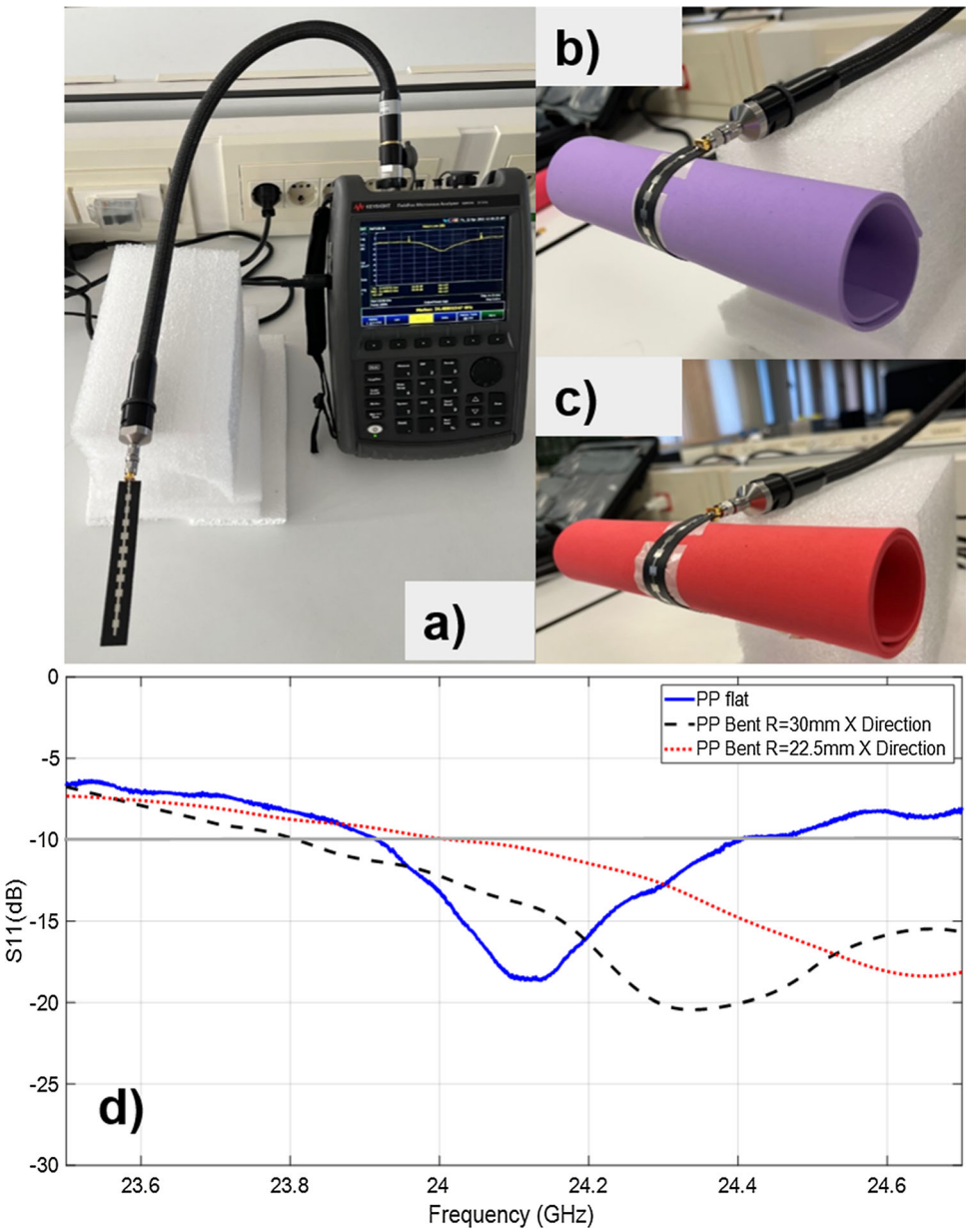

Fig. 9 Measurement set-up and S11 (dB) results for the array antenna on PP under flat and bent conditions: **a** set-up for flat conditions, **b** using a mauve foam cylinder of radius R = 30 mm and **c** red foam cylinder of radius R = 22.5 mm; **d** measurement results (Color figure online)

higher SLL. It overcomes [73] in terms of HPBW for Phi = 90° while providing very similar G, and SLL. It outperforms [71] in radiation efficiency, which is key for wearable devices. It also doubles the gain and triples the radiation efficiency of a paper based eco-friendly design [74] which is less robust and technologically advantageous (due to multi-layered design). It provides double gain than [75] while providing lower SLL.

7 Conclusions

A flexible, compact, low-cost, 1 × 10 series-fed array antenna on PP with suitable Gain, SLL and HPBW for collision avoidance radar applications in the 24.05–24.25 GHz is achieved.

The reduced FTBR, the high radiation efficiency as well as the resulting outline dimensions and flexibility, probe the antenna suitability for wearable applications.

Table 5 Size, relative dielectric permittivity, bandwidth and impedance matching

Ref.	Elements	Size (mm^3)	ε_r	BW (GHz)	BW (%)	S11 (dB)
[59]	1 × 8	89 × 21.5 × 0.254	3.66	0.25	1.0	-20
[60]	6 × 8	50 × 59 × 0.254	3.66	0.25	1.0	–
[61]	1 × 4	60 × 30 × 1.6	4.4	2.9	12	− 23
[62]	12 × 1 × 8	135 × 58.7 × 0.254	3.6	0.65	2.7	− 20
[63]	1 × 6	47.2 × 34.4 × 0.81	3.38	1.5	6.9	− 30
[64]	1 × 4	23.9 × 14.4 × 0.203	3.38	16	49.7	
[64]	1 × 6	67 × 16.5 × 0.254	3.48	0.40	1.5	− 12
[66]	8 × 8	50 × 50 × 0.754	3.66	1.5	6.3	− 27
[67]	2 × 8	74.9 × 74.9 × 3.3	–	0.2	1.0	− 8
[68]	2 × 2	29 × 21 × 0.254	3.48	0.51	2.1	− 35
[69]	1 × 5	90 × 25 × 0.203	3.55	0.39	1.6	− 25
[70]	2 × 1	26.7 × 20.4 × 0.8	3.0	1.71	7.1	− 45
[71]	2 × 24	230 × 31 × 0.254	2.17	0.39	1.6	− 20
[72]	4 × 4	24 × 21 × 43.3	2.2	2.75	11.7	− 38
[73]	1 × 10	160 × 43.2 × 0.5	2.3	0.32	1.3	− 20
[74]	2 × 2	20 × 20 × 0.68	2.9	2.0	8.3	− 35
[75]	1 × 6	32.4 × 15 × 1.016	2.2	2	8.0	− 28
This work on PP	1 × 10	98.7 × 14.4 × 0.52	2.2	0.28	1.2	− 25

Table 6 Radiation properties

Ref.	G (dBi)	η (%)	SLL (dB) φ = 0°	HPBW (°) φ = 0°	SLL (dB) φ = 90°	HPBW (°) φ = 90°
[59]	12.2	58.8	− 29.4	14	− 28.2	75
[60]	20.6	–	− 18	19.2	− 19	12.2
[61]	9.7	–	–	–	–	–
[62]	24.2	–	− 23	12.5	− 23	5.6
[63]	9.5	–	− 25	80	− 12	90
[64]	9.12	–	− 15	24	–	187
[65]	13	–	− 26	17.5	–	–
[66]	20.9	–	− 21	15	− 22	28
[67]	17	–	− 20	12	− 20	50
[68]	10.4	–	–	58.5	–	47.5
[69]	11	–	− 20	82	− 10	17
[70]	9.2	99	**− 20**	60	− 10	30
[71]	21.7	60	− 21	3.6	− 21	46
[72]	20.6	88	− 15	15	− 15	15
[73]	17	–	− 18	8.2	− 18	80
[74]	7.4	35	–	54	− 25	48
[75]	8	–	− 10	60	− 20	30
This work on PP	16.8	91	− 18	9.2	− 25	64

It has been shown that PP can be used to manufacture antennas in the 24 GHz mm band with conventional techniques. Moreover, its eco-friendliness reduces the environmental footprint of electronic devices and paves the way to circular economy.

Author contributions MEDCG: conceptualization, methodology, data curation, formal analysis, investigation, validation, writing–original draft preparation and visualization, writing–review and editing, supervision and funding acquisition. HFÁ: investigation, validation, writing–review. FL-HA: funding acquisition and supervision. All the authors read and approved the final manuscript.

Funding Open Access funding provided thanks to the CRUE-CSIC agreement with Springer Nature. This research was funded by Ministerio de Ciencia, Innovación y universidades of Spanish Government under project META-IMAGER PID2021-122697OB-I00 and by Gobierno del Principado de Asturias under project IDI/2021/000097.

Data availability The datasets generated during and/or analysed during the current study are available from the corresponding author on reasonable request.

Declarations

Conflict of interest All authors declare that they have no conflicts of interest.

References

1. Scalise, L., et al. (2012). Experimental investigation of electromagnetic obstacle detection for visually impaired users: A comparison with ultrasonic sensing. *IEEE Transactions on Instrumentation and Measurement, 61*(11), 3047–3057. https://doi.org/10.1109/TIM.2012.2202169
2. Strada, J. (2016). *Visually impaired: Assistive technologies challenges and coping strategies*. Nova Science Pub Inc.
3. Abreu, D., Toledo, J., Codina, B., & Suárez, A. (2021). Low-cost ultrasonic range improvements for an assistive device. *Sensors, 21*(12), 4250. https://doi.org/10.3390/s21124250
4. Cardillo, E., & Caddemi, A. (2019). Insight on electronic travel aids for visually impaired people: A review on the electromagnetic technology. *Electronics, 8*, 1281. https://doi.org/10.3390/electronics8111281
5. Cardillo, G. E., Li, C., & Caddemi, A. (2022). Millimeter-wave radar cane: A blind people aid with moving human recognition capabilities. *IEEE Journal of Electromagnetics, Rf and Microwaves in Medicine and Biology, 6*(2), 204–211. https://doi.org/10.1109/JERM.2021.3117129
6. Plikynas, D., Zvironas, A., Gudauskis, M., Budrionis, A., Daniusis, P., & Sliesoraityté, I. (2020). Research advances of indoor navigation for blind people: A brief review of technological instrumentation. *IEEE Instrumentation & Measurement Magazine, 23*(4), 22–32. https://doi.org/10.1109/MIM.2020.9126068
7. Zvironas, A., Gudauskis, M., & Plikynas, D. (2019). Indoor electronic traveling aids for visually impaired: Systemic review. *International Conference on Computational Science and Computational Intelligence (CSCI), 2019*, 936–942. https://doi.org/10.1109/CSCI49370.2019.00178
8. Long, N., Yan, H., Wang, L., Li, H., & Yang, Q. (2022). Unifying obstacle detection, recognition, and fusion based on the polarization color stereo camera and LiDAR for the ADAS. *Sensors, 22*, 2453. https://doi.org/10.3390/s22072453
9. Di Mattia, V., et al. (2014). An electromagnetic device for autonomous mobility of visually impaired people. In *2014 44th European Microwave Conference* (pp. 472–475). https://doi.org/10.1109/EuMC.2014.6986473
10. Kwiatkowski, P., Jaeschke, T., Starke, D., Piotrowsky, L., Deis, H., & Pohl, N. (2017). A concept study for a radar-based navigation device with sector scan antenna for visually impaired people. *First IEEE MTT-S International Microwave Bio Conference (IMBIOC), 2017*, 1–4. https://doi.org/10.1109/IMBIOC.2017.7965796
11. Gao, Y., Ghasr M. T., & Zoughi, R. (2018). Effects of translational position error on microwave synthetic aperture radar (SAR) imaging systems. In *2018 IEEE international instrumentation and measurement technology conference (I2MTC)* (pp. 1–6). https://doi.org/10.1109/I2MTC.2018.8409556
12. Álvarez, H. F., ÁLvarez-Narciandi, G., Las-Heras, F., & Laviada, J. (2021). System based on compact mmWave radar and natural body movement for assisting visually impaired people. *IEEE Access, 9*, 125042–125051. https://doi.org/10.1109/ACCESS.2021.3110582
13. Klotz, M., & Rohling, H. (2001). A 24 GHz short range radar network for automotive applications, In *2001 CIE International Conference on Radar Proceedings (Cat No.01TH8559), Beijing, China* (pp. 115–119). https://doi.org/10.1109/ICR.2001.984635
14. Ju, Y., Jin, Y., & Lee, J. (2014). Design and implementation of a 24 GHz FMCW radar system for automotive applications. *International Radar Conference Lille, 2014*, 1–4. https://doi.org/10.1109/RADAR.2014.7060385
15. Richards, M. A., Scheer, J. A., Holm, W. A. (2010). Principles of modern radar: Basic principles, SciTech Publishing-An Imprint of the IET 379 Thornall Street Edison, NJ 08837, ISBN: 978-1-891121-52-4.
16. Skolnik, M. L. (2001). *Introduction to radar systems* (3rd ed.). McGraw-Hill.
17. Heuel, S., & Rohling, H. (2010). Pedestrian recognition based on 24 GHz radar sensors. In *11-th International Radar Symposium* (pp. 1–6).
18. Peng, Z., Muñoz-Ferreras, J., Gómez-García, R., Ran, L., & Li, C. (2016). 24-GHz biomedical radar on flexible substrate for ISAR imaging. *IEEE MTT-S International Wireless Symposium (IWS), 2016*, 1–4. https://doi.org/10.1109/IEEE-IWS.2016.7585400
19. ETSI EN 302 288-1. (2005). Electromagnetic compatibility and Radio Spectrum Matters (ERM); Short Range Devices; Road Transport and Traffic Telematics (RTTT); Short range radar equipment operating in the 24 GHz range; Part 1: Technical requirements and methods of measurement. European Telecommunications Standards Institute.
20. Xiang, Yi., & Fang, G. (2019). Liang Cheng Wang, Liu Bei, Chenyang Li, Kaituo Yang, Chirn Chye and Quan Xue, A dual band 24 / 77 GHz receiver for automotive radar applications. *IEEE Access, 7*, 48053–48059. https://doi.org/10.1109/ACCESS.2019.2904493
21. Dewantari, A., Jeon, S., Kim, S., Kim, S., Kim, J., & Ka, M. (2016). Comparison of array antenna designs for 77GHz radar applications. In *Progress in Electromagnetic Research Symposium (PIERS)*, pp. 1092–1096.
22. Balanis, C. A. (2016). *Antenna theory analysis and design* (4th ed.). Wiley.
23. Pozar, D. M., & Schaubert, D. H. (1995). Microstrip antenna array design. *Microstrip antennas: The analysis and design of microstrip antennas and arrays* (pp. 267–308). IEEE.

24. Yin, J., Wu, Q., Yu, C., Wang, H., & Hong, W. (2017). Low-sidelobe-level series-fed microstrip antenna array of unequal interelement spacing. *IEEE Antennas and Wireless Propagation Letters, 16*, 1695–1698. https://doi.org/10.1109/LAWP.2017.2666427
25. Dolph, C. L. (1946). A current distribution for broadside arrays which optimizes the relationship between beam width and side-lobe level. *Proceedings of the IRE, 34*, 335–348.
26. Lau, B., & Leung, Y. (1999). Analysis of Dolph-Chebyshev patterns for uniform linear arrays. SPL-TR-013, ATRI, Curtin Uni of Tech, 181–185.
27. Tseng, C. Y., & Griffiths, L. J. (1992). A simple algorithm to achieve desired patterns for arbitrary arrays. *IEEE Transaction Signal Processing, 40*, 2737–2746.
28. Babas, D., & Sahalos, J. (2007). Synthesis method of series-fed microstrip antenna arrays. *Electronics Letters, 43*(2), 78–80. https://doi.org/10.1049/el:20073391
29. Otto, S., Chen, Z. (2009). A taper optimization for pattern synthesis of microstrip series-fed patch array antennas. In *Proceedings of the IEEE EuWIT conference.*
30. Kothapudi, V. K., & Kumar, V. (2019). SFCFOS uniform and Chebyshev amplitude distribution linear array antenna for K-band applications. *Journal of Electromagnetic Engineering and Science, 19*(1), 64–70. https://doi.org/10.26866/jees.2019.19.1.64
31. Rogers Corp Laminates. (2022). Datasheet of the RO3003 dielectric material. https://rogerscorp.com/-/media/project/rogerscorp/documents/advanced-electronics-solutions/english/data-sheets/ro3000-laminate-data-sheet-ro3003——ro3006——ro3010——ro3035.pdf. Accessed on 18 September 2022.
32. Directive 2011/65/EU of the European Parliament and of the Council. (2022). https://eur-lex.europa.eu/legalcontent/EN/TXT/PDF/?uri=CELEX:32011L0065&from=EN. Accessed on 18 September 2022.
33. Alsabri, A., Furqan, T., & Al-Ghamdi, S. G. (2022). Environmental impacts of polypropylene (PP) production and prospects of its recycling in the GCC region. *Materials Today: Proceedings, 56*, 2245–2251.
34. Suksiripattanapong, C., Phetprapai, T., Singsang, W., Phetchuay, C., Thumrongvut, J., & Tabyang, W. (2022). Utilization of recycled plastic waste in fiber reinforced concrete for eco-friendly footpath and pavement applications. *Sustainability, 14*, 6839. https://doi.org/10.3390/su14116839
35. Bora, R. R., Wang, R., & You, F. (2020). Waste polypropylene plastic recycling toward climate change mitigation and circular economy: Energy. *Environmental and Technoeconomic Perspectives, ACS Sustainable Chemical Engineering, 8*(43), 16350–16363.
36. Galve, J. E., Elduque, D., Pina, C., & Javierre, C. (2022). Life cycle assessment of a plastic part injected with recycled polypropylene: A comparison with alternative virgin materials. *International Journal of Precision Engineering and Manufacturing-Green Technology., 9*, 919–932. https://doi.org/10.1007/s40684-021-00363-2
37. de Cos, M. E., & Las-Heras, F. (2013). Polypropylene-based dual-band CPW-fed monopole antenna [antenna appcations corner]. *IEEE Antennas and Propogation Magazine, 55*(3), 264–273. https://doi.org/10.1109/MAP.2013.6586683
38. Garcia-Gamez, L., Bernard, L., Collardey, S., Covic, H., Sauleau, R., Mahdjoubi, K., Potier, P., & Pouliguen, P. (2019). Compact GNSS metasurface-inspired cavity antennas. *IEEE Antennas and Wireless Propagation Letters, 18*(12), 2652–2656. https://doi.org/10.1109/LAWP.2019.2947791
39. Campo, C., Bernard, L., Boeglen, H., Hengy, S., & Paillot, J. (2018). Software-defined radio system for tracking application. In *12th European conference on antennas and propagation (EuCAP 2018)* (pp. 1–5). https://doi.org/10.1049/cp.2018.0582
40. Causse, A., Rodriguez, K., Bernard, L., Sharaiha, A., & Collardey, S. (2021). Compact bandwidth enhanced cavity-backed magneto-electric dipole antenna with outer γ-shaped probe for GNSS bands. *Sensors, 21*(11), 3599. https://doi.org/10.3390/s21113599
41. Causse, A., Bernard, L., Collardey, S., & Sharaiha, A. (2021). Small CP cavity-backed magneto-electric antenna with parasitic elements for GNSS applications. In *15th European conference on antennas and propagation (EuCAP)* (pp. 1–5). https://doi.org/10.23919/EuCAP51087.2021.9411228
42. Garcia-Gamez, L., Bernard, L., Sauleau, R., Collardey, S., Mahdjoubi, K., Pouliguen, P., et al. (2022). Circularly-polarized GNSS metasurface antenna with two feed points in a sub-wavelength metallic cavity. In *16th European conference on antennas and propagation (EuCAP), Madrid, Spain* (pp. 1–4). https://doi.org/10.23919/EuCAP53622.2022.9769030
43. Bernard, L., Campo C., & Roussel, E. (2023). Eco-friendly based substrates for telemetry antennas in UHF- and S-bands. In *2023 17th European conference on antennas and propagation (EuCAP), Florence, Italy* (pp. 1–5). https://doi.org/10.23919/EuCAP57121.2023.10133806
44. Application Note. (2018). Keysight 85072A 10GHz Split Cylinder Resonator, Technical Overview, literature number 5989–6182EN. Retrieved December 2022 from https://www.keysight.com/us/en/assets/7018-01496/technical-overviews/5989-6182.pdf
45. Baker-Jarvis, J., Janezic, M. D., & Degroot, D. C. (2010). High-frequency dielectric measurements. *IEEE Instrumentation & Measurement Magazine, 13*(2), 24–31. https://doi.org/10.1109/MIM.2010.5438334
46. Application Note. (2020). Basics of measuring the dielectric properties of materials. Keysight Technologies. Retrieved January 2023 from https://www.keysight.com/us/en/assets/7018-01284/application-notes/5989-2589.pdf
47. Application Note. (2020). N1501A Dielectric probe kit 10 MHz to 50 GHz. Keysight Technologies. Retrieved December 2022 from https://www.keysight.com/us/en/assets/7018-04631/technical-overviews/5992-0264.pdf
48. Application Note. (2017). Split post dielectric resonators for dielectric measurements of substrates, literature number 5989–5384EN. Keysight Technologies. Retrieved January 2023 from https://www.keysight.com/us/en/assets/7018-01416/application-notes/5989-5384.pdf
49. Skocik, P., & Neumann, P. (2015). Measurement of complex permittivity in free space. *Procedia Engineering, 100*, 100–104. https://doi.org/10.1016/j.proeng.2015.01.347
50. Pérez-Escribano, M., & Márquez-Segura, E. (2021). Parameters characterization of dielectric materials samples in microwave and millimeter-wave bands. *IEEE Transactions on Microwave Theory and Techniques, 69*(3), 1723–1732. https://doi.org/10.1109/TMTT.2020.3045211
51. Pérez-Escribano, M., & Márquez-Segura, E. (2021). Random errors in broadband characterization of the propagation constant of transmission lines using multiple two-port measurements. *IEEE Access, 9*, 59038–59047. https://doi.org/10.1109/ACCESS.2021.3073173
52. Latti, K. P., Kettunen, M., Strom, J., & Silventoinen, P. (2007). A review of microstrip T-Resonator method in determining the dielectric properties of printed circuit board materials. *IEEE Transactions on Instrumentation and Measurement, 56*(5), 1845–1850. https://doi.org/10.1109/TIM.2007.903587
53. Vorlíček, J., Rusz, J., Oppl, L., & Vrba, J. (2010). Complex permittivity measurement of substrates using ring resonator. In *Technical computing Bratislava.* https://www2.humusoft.cz/www/papers/tcb10/107_vorlicek.pdf

54. Thompson, D., Falah, M., Fang, X., & Linton, D. (2003). Dielectric characterization using the microstrip resonator method. In *2003 high frequency postgraduate student colloquium (Cat. No.03TH8707), Belfast, Ireland* (pp. 23–26). https://doi.org/10.1109/HFPSC.2003.1242298
55. Metzler, T. (1981). Microstrip series arrays. *IEEE Transactions on Antennas and Propagation, 29*(1), 174–178.
56. IEEE Recommended Practice for Antenna Measurements. (2022). In *IEEE Std 149-2021 (Revision of IEEE Std 149-1977)* (pp.1–207). https://doi.org/10.1109/IEEESTD.2022.9714428
57. Krauss, J. D. (1988). *Antennas*. New York: McGraw Hill.
58. Elliot, R.S. (1964). Beamwidth and directivity of large scanning arrays. *The Microwave Journal*, pp. 74–82.
59. Qian, J., Zhu, H., Tang, M., & Mao, J. (2021). A 24 GHz microstrip comb array antenna with high sidelobe suppression for radar sensor. *IEEE Antennas and Wireless Propagation Letters, 20*(7), 1220–1224. https://doi.org/10.1109/LAWP.2021.3075887
60. Chen, Y., Liu, Y., Zhang, Y., Yue, Z., & Jia, Y. (2019). A 24GHz millimeter wave microstrip antenna array for automotive radar. In *International Symposium on Antennas and Propagation (ISAP)* (pp.1–2).
61. Banuprakash, R., Hebbar, H.G., Janani, N., Raghav, K.K., & Sudha, M. (2020). Microstrip array antenna for 24GHz automotive RADAR. In *7th international conference on smart structures and systems (ICSSS)* (pp. 1–6).
62. Jia, Y., Liu, Y., & Zhang, Y. (2020). A 24 GHz microstrip antenna array with large space and narrow beamwidth. *Microwave and Optical Technology Letters, 62*, 1615–1620. https://doi.org/10.1002/mop.32190
63. Chaudhuri, S., Mishra, M., Kshetrimayum, R. S., Sonkar, R. K., Chel, H., & Singh, V. K. (2020). Rectangular DRA array for 24 GHz ISM-band applications. *IEEE Antennas and Wireless Propagation Letters, 19*(9), 1501–1505. https://doi.org/10.1109/LAWP.2020.3007585
64. Chen, Y., Shi, J., Xu, K., Lin, L., & Wang, L. (2023). A compact wideband Quasi-Yagi antenna for millimeter-wave communication. *IEEE Antennas and Wireless Propagation Letters, 22*(6), 1481–1485. https://doi.org/10.1109/LAWP.2023.3247429
65. Jin, H., Zhu, L., Liu, X., & Yang, G. (2018). Design of a microstrip antenna array with low side-lobe for 24GHz radar sensors. *International Conference on Microwave and Millimeter Wave Technology (ICMMT), 2018*, 1–3.
66. Yang, W., Yang, Y., Che, W., Gu, L., & Li, X. (2016). A novel 24-GHz series-fed patch antenna array for radar system. *IEEE International Workshop on Electromagnetics: Applications and Student Innovation Competition (iWEM), 2016*, 1–4. https://doi.org/10.1109/iWEM.2016.7505065
67. SAM-2432431750-KF-L1. K band microstrip patch array antenna. https://sftp.eravant.com/content/datasheets/SAM-2432431750-KF-L1.pdf
68. Kim, S., Kim, D. K., Kim, Y., Choi, J., & Jung, K. (2019). A 24 GHz ISM-band doppler radar antenna with high isolation characteristic for moving target sensing applications. *IEEE Antennas and Wireless Propagation Letters, 18*(7), 1532–1536. https://doi.org/10.1109/LAWP.2019.2922008
69. Kuo, C.-H., Lin, C.-C., & Sun, J.-S. (2017). Modified microstrip franklin array antenna for automotive short-range radar application in blind spot information system. *IEEE Antennas and Wireless Propagation Letters, 16*, 1731–1734. https://doi.org/10.1109/LAWP.2017.2670231
70. Flórez Berdasco, A., de Cos Gómez, M. E., Fernández Álvarez, H., & Las-Heras Andrés, F. (2023). Millimeter wave array-HIS antenna for imaging applications. *Applied Physics: A, 129*, 397. https://doi.org/10.1007/s00339-023-06676-0
71. Slovic, M., Jokanovic, B., & Kolundzija, B. (2005). High efficiency patch antenna for 24 GHz anticollision radar. *TELSIKS 2005-International Conference on Telecommunication in Modern Satellite Cable and Broadcasting Services, 1*, 20–23.
72. He, Y., Ma, K., Yan, N., Wang, Y., & Zhang, H. (2023). 3-D SISL feeding network for 2-D cavity-backed endfire dipole array at 24 GHz. *IEEE Antennas and Wireless Propagation Letters, 22*(5), 990–994. https://doi.org/10.1109/LAWP.2022.3229841
73. Jung, Y., Park, D., & Jung, C. W. (2010). Low cost 24GHz patch array antenna for high sensitivity EM sensor. *Asia-Pacific Microwave Conference, 2010*, 2208–2211.
74. Poggiani, M., Mezzanotte, P., Mariotti, C., Virili, M., Orecchini, G., Alimenti, F., et al. (2014). 24 GHz patch antenna network in cellulose-based materials for green wireless internet applications. *Science measurement and Technology IET, 8*(6), 342–349. https://doi.org/10.1049/iet-smt.2013.0279
75. Zhou, H., Geng, J., & Jin, R. (2022). A magnetic Yagi-Uda antenna with vertically polarized endfire radiation in millimeter-wave band applying higher order mode. *IEEE Transactions on Antennas and Propagation, 70*(10), 8941–8950. https://doi.org/10.1109/TAP.2022.3177476

María Elena de Cos Gómez received the Telecommunication Engineering Degree and the Ph.D. degree from the University of Cantabria, Santander, Spain, in 2002 and 2006, respectively. She was a Researcher Engineer in collaboration with ACORDE S.A, Santander, from 2004 to 2007. In 2007, she joined the Área de Teoría de la Señal y Comunicaciones, Universidad de Oviedo, Gijón, Spain. She was a visiting researcher in IETR Rennes, France in 2011 and 2014. Her current research interests include metamaterials design and its applications to antennas and microwave circuits, the design of antennas for wearable and RFID systems, radar cross section (RCS) reduction, location techniques, and wireless sensor networks design and applications. She has participated in a great number of research projects and has authored and co-authored over 75 journal and conference contributions. She was awarded as an outstanding IEEE AWPL reviewer (2017–2018). Dr. de Cos Gómez is an Associate Editor of IEEE Antennas and Wireless Propagation Letters from 2018.

Humberto Fernández Álvarez received the M.S. and Ph.D. degrees in telecommunication engineering from the University of Oviedo, in 2014 and 2019. Mr. Álvarez received the Best Final Degree Research Project Award from Cátedra Telefónica in 2015 and a Research Contract from the University of Oviedo. He was a visiting researcher in the Wireless Communications Research Group (WiCR) of the Loughborough University in 2019. He was awarded COIT-AEIT best doctoral Thesis in Satellite Communication Systems by Hispasat company-XL edition and also to the best doctoral thesis (Engineering) at University of Oviedo, 2019. His research interests include metamaterial absorbers, metasurfaces (frequency selective surfaces and artificial magnetic conductors), antenna design and propagation, computational electromagnetics, and measurement techniques.

Fernando Las-Heras Andrés (Senior Member, IEEE) received the M.S. and Ph.D. degrees in telecommunication engineering from the Technical University of Madrid (UPM), Madrid, Spain, in 1987 and 1990, respectively. From 1988 to 1990, he was a National Graduate Research Fellow with UPM, where he was an Associate Professor with the Department of Signal, Systems and Radiocommunications, from 1991 to 2000. Since December 2003, he has been a Full Professor with the University of Oviedo, Gijón, Spain, where he was the Vice-Dean of telecommunication engineering with the Technical School of Engineering from 2004 to 2008. He was a Visiting Lecturer with the National University of Engineering, Rímac, Peru, in 1996; a Visiting Researcher with Syracuse University, Syracuse, NY, in 2000; and a Short-Term Visiting Lecturer with ESIGELEC, Saint-Étiennedu-Rouvray, France, from 2005 to 2011. He was the Telefónica Chair of "RF Technologies," "Information and Communications Technologies (ICTs) applied to Environment," and "ICTs and Smartcities" with the University of Oviedo from 2005 to 2015. He has been the Head of the Research Group Signal Theory and Communications TSC-UNIOVI, Department of Electrical Engineering, University of Oviedo, since 2001. He has led and participated in a great number of research projects and has authored over 230 articles published in indexed scientific journals on topics of antennas, propagation, metamaterials, and inverse problems with application to antenna measurement, electromagnetic (EM) imaging, and localization, developing computational EMs algorithms and technology on microwaves, millimeter wave, and terahertz (THz) frequency bands. Dr. Las-Heras was a member of the Board of Directors of the IEEE Spain Section from 2012 to 2015, a member from 2016 to 2017 and a Vice-President from 2020 to 2022 of the Board of the Joint IEEE Microwave Theory and Techniques Society (MTT-S) and Antennas and Propagation Society (AP-S) Spain Chapter, a member of the Science, Technology and Innovation Council of Asturias from 2010 to 2012, and a President of the Professional Association of Telecommunication Engineers, Asturias, Spain.